Mobile small bipolarons on a three-dimensional cubic lattice

A. R. Davenport,[1] J. P. Hague,[1] and P. E. Kornilovitch[2]
[1]*Department of Physical Sciences, The Open University, Walton Hall, Milton Keynes MK7 6AA, United Kingdom*
[2]*Hewlett-Packard Company, 1070 NE Circle Boulevard, Corvallis, Oregon 97330, USA*
(Received 6 January 2012; published 5 July 2012)

We use numerically exact quantum Monte Carlo (QMC) to compute the properties of three-dimensional bipolarons for interaction strengths where perturbation theory fails. For intermediate electron-phonon coupling and Hubbard U, we find that bipolarons can be both small and light, a prerequisite for bipolaron superconductivity. We use the QMC results to make estimates of transition temperatures, which peak at between 90–120 K and are demonstrated to be insensitive to Coulomb repulsion and impurities.

DOI: 10.1103/PhysRevB.86.035106 PACS number(s): 71.38.Mx, 71.38.Fp

I. INTRODUCTION

The mechanisms of three-dimensional superconductors with high transition temperatures (such as the bismuthates) are widely acknowledged to have their origins in the electron-phonon interaction. In at least some materials, a proposed mechanism involves the pairing of phonon dressed electrons (polarons) to form bipolarons. At sufficiently low temperatures, these bipolarons form a Bose-Einstein condensate with superconducting properties.[1] The main criteria for bipolaronic superconductivity with significant transition temperatures are bipolaron mobility (low effective mass)[2] with sufficient density (small bipolarons). Although small (bi)polarons are often viewed as immobile states that may be easily localized by disorder, small mobile bipolarons that can lead to superconductivity with high transition temperatures have been found in one and two dimensions.[2–4]

Polarons occur naturally in nearly all media, from plasmas and ultracold atoms through normal bulk materials and possibly high-temperature superconductors.[3,5] Landau introduced the polaron concept in 1933 to study lattice polarization due to the motion of electrons through ionic solids:[6] An electron moving though a crystal lattice creates distortions that follow its trajectory, producing a phonon cloud that propagates though the system, surrounding the electron.[3,7]

Bipolarons are formed when two polarons interact with each other using phonon-mediated interactions to form pairs. These pairs can be strongly bound and travel though the lattice as a single composite particle. There are many different interaction types that lead to bipolaron creation.[8] In this paper, we consider an extended Hubbard-Holstein model, where the Coulomb interaction is purely onsite, and an extended-Holstein interaction couples the electron density to lattice vibrations on the same site and near-neighbor sites, similar to the interaction introduced by Bonča and Trugman.[8,9] Increasing this intersite interaction allows electrons to form bipolarons and overcomes the Coulomb repulsion so that large bipolarons become local (small) bipolarons with approximately the size of the lattice constant.[10] The site-local Holstein model describes an extreme short-range limit where electrons can form pairs on single atoms. In this case, the electron-phonon interaction has to overcome the onsite repulsion to form a bipolaron.[11] We note that the interactions used here are distinct from the specific forms required to describe bismuthate superconductors.[12]

Recent studies of low-dimensional bipolarons have utilized various numerical methods and analytical techniques. One-dimensional bipolarons have been found to be relevant in describing strong electron-phonon interactions in low-dimensional organic semiconductors,[13] and it is possible that three-dimensional (3D) bipolarons in a strong magnetic field simplify into one-dimensional (1D) bipolarons.[14] Two-dimensional (2D) bipolarons have been investigated extensively in the study of two-dimensional conductors and high-temperature superconductors such as the cuprates.[1]

Properties of the short-range Hubbard-Holstein bipolaron model have been established on small lattices using exact diagonalization[11] and an optimized approach for exact diagonalization at weak coupling.[15] Advanced variational techniques,[16] density-matrix renormalization-group,[17] and various quantum Monte Carlo (QMC) approaches[7,18] have all been used to study 2D bipolaron systems. It is found in one dimension that only a small attractive force between electrons leads to pairing, the most important factor being the nearest-neighbor interaction when considering long-ranged interactions.[7,19] Two-dimensional work also shows us that inclusion of nearest-neighbor interaction is responsible for significant change compared with the Hubbard-Holstein model.[8,20] Light bipolarons are found on a simple square lattice, showing that elaborate lattices are not needed to create small light pairs that have the potential to form Bose condensates.[8] On change of dimension from 1D to 2D, an increase in electron-phonon coupling constant and nearest-neighbor attraction is needed to create onsite bipolarons.[7,8]

There have been several notable studies of 3D bipolarons, especially in relation to superconductors, to understand the reasons why cuprates and other layered superconductors are different to 3D materials.[21,22] Several publications have examined the differences between the binding of bipolarons in two and three dimensions, concluding that a greater attraction is needed to form stable bipolarons on 3D lattices.[23,24] It has been found that the probability of bipolaron formation increases with decreasing dimensions or increase in the crystal anisotropy.[25] Variational studies of the region of existence of the three-dimensional singlet bipolaron have allowed investigation of the relationship between the critical value of the electron-phonon coupling constant and the dielectric properties of the medium,[26] concluding that conditions in alkali-halide crystals are not suitable even for metastable

 ©2012 American Physical Society

bipolarons and that three-dimensional continuum bipolarons do not exist in La_2CuO_4. However, metal-ammonia systems potentially lie within the region of existence for three-dimensional continuum bipolarons.[26] In the context of 3D polarons, we have also examined binding to attractive impurities, showing that polarons are localized when the impurity potential is around four effective hoppings in magnitude.[27]

The work presented here goes beyond previous work by considering exact solutions for 3D extended Hubbard-Holstein bipolarons (both numerical and analytic). Exact solutions are important to understand regions of the parameter space where perturbative approximations break down, and as we will show are essential for understanding the regions where bipolaronic superconductivity is strongest. The paper is organized as follows: In Sec. II, we introduce the model. The Lang-Firsov transformation is performed before a brief overview of the continuous-time quantum Monte Carlo (CTQMC) simulation method. Section III presents quantum Monte Carlo results for singlet bipolaron properties, including total energy, number of associated phonons, inverse mass, and average bipolaron size. Finally, in Sec. IV, we look at the possibility of Bose-Einstein condensation of three-dimensional bipolarons. For completeness, in the Appendix, we consider the U-V model corresponding to the high phonon-frequency limit. Solving the equation analytically, we find the binding conditions for varying onsite attraction U and nearest-neighbor repulsion V.

II. MODEL AND METHODS

A. Model

The extended Hubbard-Holstein model used here has its basis in a general electron-phonon Hamiltonian with electrostatic repulsion, which is written in the following form:[7,8]

$$H = -t\sum_{\langle \mathbf{nn}'\rangle,\sigma} c^{\dagger}_{\boldsymbol{n}',\sigma}c_{\boldsymbol{n},\sigma} + \frac{1}{2}\sum_{\boldsymbol{nn}'\sigma\sigma'} v(\boldsymbol{n},\boldsymbol{n}')c^{\dagger}_{\boldsymbol{n}\sigma}c_{\boldsymbol{n}\sigma}c^{\dagger}_{\boldsymbol{n}'\sigma'}c_{\boldsymbol{n}'\sigma'} + \sum_{\boldsymbol{m}}\frac{\hat{P}^2_{\boldsymbol{m}}}{2M} + \sum_{\boldsymbol{m}}\frac{\xi^2_{\boldsymbol{m}}M\omega^2}{2} - \sum_{\boldsymbol{nm}\sigma} f_{\boldsymbol{m}}(\boldsymbol{n})c^{\dagger}_{\boldsymbol{n}\sigma}c_{\boldsymbol{n}\sigma}\xi_{\boldsymbol{m}}, \tag{1}$$

where $\boldsymbol{n}$ and $\boldsymbol{m}$ represent vectors to electrons and ions, respectively, c ($c^{\dagger}$) are the creation (annihilation) operators for electrons, M is the ion mass, ω is the phonon frequency, and σ is the z component of the electron spin. The first term in the equation expresses the kinetic energy of electrons moving from site to site. The element t is the hopping integral for an electron moving between neighboring sites.

The second term in the Hamiltonian represents the Coulomb repulsion v between two electrons. Here, the repulsion is approximated to have the Hubbard form, and long-ranged interactions are assumed to be insignificant due to screening in the material[28] so the repulsive term has the form $H_{\text{Hubbard}} = U\sum_n n_{i\uparrow}n_{i\downarrow}$, where U is the magnitude of the repulsion.[7,8] Note that near-neighbor interactions are in principle allowed, but neglected in Secs. III and IV of this paper.

The final three terms include the effects of lattice vibration. The ion momentum is described by the $\hat{P}_{\boldsymbol{m}}$ operator and the ion displacement is signified by $\xi_{\boldsymbol{m}}$. Here, we take $\xi_{\boldsymbol{m}}$ to be one dimensional, which is an approximation that could relate to phonon modes polarized by a strong electric field, a three-dimensional molecular crystal with molecular ordering along a single direction or possibly radial phonon modes. Following Ref. 8, we take the force function to be

$$f_{\boldsymbol{m}}(\boldsymbol{n}) = \kappa\sum_{\boldsymbol{l}_i}\delta_{\boldsymbol{n},\boldsymbol{m}+\boldsymbol{l}_i/2}. \tag{2}$$

This describes interaction between electrons on sites at vectors $\boldsymbol{n}$ and vibrating ions between valance sites at positions $\boldsymbol{m}$. $\boldsymbol{l}_i$ are the vectors between nearest-neighbor valence sites at $\boldsymbol{r}$ and $\boldsymbol{r}'$. An effective electron-electron interaction can be defined as

$$\Phi_{\Delta\boldsymbol{r}}[\boldsymbol{r},\boldsymbol{r}'] = \sum_{\mathrm{m}} f_{\mathrm{m}}[\boldsymbol{r}]f_{\mathrm{m}+\Delta\boldsymbol{r}}[\boldsymbol{r}'], \tag{3}$$

so that for the chosen force function, $\Phi_0[\boldsymbol{r},\boldsymbol{r}']/\Phi_0[0,0] = \gamma$ where the nearest-neighbor interaction strength (γ) strictly has the value $1/z$. The reason for $\Delta\boldsymbol{r}$ will be explained later on in the paper. Here, we will also modify γ to investigate the effects of turning on the intersite interaction. For large phonon frequency, this interaction can then be mapped directly onto a U-V model. For $\gamma = 0$, a Holstein interaction is recovered, equivalent to $f_{\boldsymbol{m}}(\boldsymbol{n}) = \kappa\delta_{\boldsymbol{mn}}$. The shift in γ is equivalent to moving the vibrating ions within the unit cell so that they get closer to the site's host electrons.

B. Lang-Firsov transformation

In the limit that phonon frequency becomes infinite, the model described in Eq. (1) can be mapped onto a U-V model, consisting of an onsite Hubbard U and inter-site Hubbard V. The mapping uses a Lang-Firsov canonical transformation,[29] which creates a new Hamiltonian $\tilde{H} = e^{-S}He^{S}$ and wave function $|\tilde{\psi}\rangle = e^{-S}|\psi\rangle$, where $\tilde{H} = H + [S,H] + [S,[S,H]] + \cdots$ and $S = \mathrm{g}n(d^{\dagger} - d)$. Here, g is a dimensionless interaction constant proportional to the force and $d^{\dagger}$ (d) is the phonon creation (annihilation) operator. Under this transformation, the creation operators for electrons and phonons become

$$\begin{aligned} c^{\dagger}_i \to \tilde{c}^{\dagger}_i &= c^{\dagger}_i\exp\left[\sum_j \mathrm{g}_{ij}(d^{\dagger}_j - d_j)\right], \\ d^{\dagger}_j \to \tilde{d}^{\dagger}_j &= d^{\dagger}_j + \sum_i \mathrm{g}_{ij}n_i. \end{aligned} \tag{4}$$

On transforming the atomic Hamiltonian ($t \to 0$), the electron and phonon subsystems are decoupled:

$$\tilde{H}_{at} = -\sum_{ii'} n_i n_{i'}\sum_j \frac{f_{ij}f_{i'j}}{2M\omega^2} + \hbar\omega\sum_j\left(d^{\dagger}_j d_j + \frac{1}{2}\right). \tag{5}$$

The function Φ_0 and a dimensionless interaction parameter $\lambda = E_p/W$ are introduced to simplify the Hamiltonian, where W is the half-bandwidth zt, and $E_p = \sum_j f^2_{0j}/2M\omega^2 = \Phi_0(0,0)/2M\omega^2$ is the polaron shift, leading to

$$\tilde{H}_{at} = -\sum_{ii'} n_i n_{i'}\frac{W\lambda\Phi_0(i,i')}{\Phi_0(0,0)} + \hbar\omega\sum_j\left(d^{\dagger}_j d_j + \frac{1}{2}\right). \tag{6}$$

Transformation of the tight-binding Hamiltonian leads to

$$\tilde{H}_{tb} = \sum_{ii'}\sigma_{ii'}c^{\dagger}_i c_{i'}, \tag{7}$$

with

$$\sigma_{ii'} = t_{ii'}\exp\left[-\frac{W\lambda}{\hbar\omega}\left(1-\frac{\Phi_0(i,i')}{\Phi_0(0,0)}\right)\right] \times \exp\left(\sum_j (g_{ij}-g_{i'j})d_j^\dagger\right)\exp\left(-\sum_j (g_{ij}-g_{i'j})d_j\right), \tag{8}$$

where $g_{ij} = f_{ij}/\omega\sqrt{2M\omega}$. When the phonon frequency is very large, the ground state contains no real phonons, and there is a further simplification leading to a modified hopping $\sigma_{ii'} \approx t'_{ii'} = t_{ii'}\exp[-\frac{W\lambda}{\hbar\omega}(1-\frac{\Phi_0(i,i')}{\Phi_0(0,0)})]$. Exact solutions of the transformed Hamiltonian in the large phonon frequency limit can be found in the Appendix for comparison with the numerical results.

C. Computational methods

We use the continuous-time quantum Monte Carlo method, which has been used to simulate the screened Hubbard-Fröhlich bipolaron in 1D and 2D.[7,30] A more in-depth overview of our algorithm has been presented in a previous paper and so will not be repeated.[8] The continuous-time quantum Monte Carlo algorithm is based on path integrals, where each path $\mathbf{r}_i(\tau)$ exists in imaginary time and represents a single particle in the system. The algorithm probes path configurations which are each assigned a weight $\exp(A)$ where

$$A[\boldsymbol{r}] = \frac{z\lambda\bar{\omega}}{2\Phi_0(0,0)}\int_0^{\bar{\beta}}\int_0^{\bar{\beta}} d\tau\, d\tau' e^{\frac{-\bar{\omega}\bar{\beta}}{2}} \sum_{ij}\Phi_0[\boldsymbol{r}_i(\tau),\boldsymbol{r}_j(\tau')](e^{\bar{\omega}(\frac{\bar{\beta}}{2}-|\tau-\tau'|)}+e^{-\bar{\omega}(\frac{\bar{\beta}}{2}-|\tau-\tau'|)}) + \frac{z\lambda\bar{\omega}}{\Phi_0(0,0)}\int_0^{\bar{\beta}}\int_0^{\bar{\beta}} d\tau\, d\tau' e^{-\bar{\omega}\tau}e^{-\bar{\omega}(\bar{\beta}-\tau')}\sum_{ij}(\Phi_{\Delta\boldsymbol{r}}[\boldsymbol{r}_i(\tau),\boldsymbol{r}_j(\tau')]-\Phi_0[\boldsymbol{r}_i(\tau),\boldsymbol{r}_j(\tau')]) - \frac{1}{2}\int_0^{\beta} v[\boldsymbol{r}_1(\tau),\boldsymbol{r}_2(\tau)]d\tau. \tag{9}$$

Here, $\Delta\boldsymbol{r} = \boldsymbol{r}(\beta)-\boldsymbol{r}(0)$ is the distance between the end points of the paths in the nonexchange configuration, the phonon frequency $\bar{\omega} = \hbar\omega/t$, and inverse temperature $\bar{\beta} = t/k_BT$. $i = 1,2$ and $j = 1,2$ represent the fermion paths. $v(\boldsymbol{r}_1,\boldsymbol{r}_2) = U\delta_{\boldsymbol{r}_1,\boldsymbol{r}_2}$ is an instantaneous Hubbard repulsion between electrons. The paths lie between the range $\tau \in 0,\beta$, and are formed from straight segments punctuated with "kinks" representing site-to-site hopping. The algorithm is used to compute (bi)polaron energy, the number of phonons in the system, the effective mass of the (bi)polaron, and the radius of the bipolaron.

III. QUANTUM MONTE CARLO AND INTERMEDIATE PHONON FREQUENCY

Using a continuous-time quantum Monte Carlo code, we simulated the extended Hubbard-Holstein model with nearest-neighbor interaction strengths of $\gamma = 0$, 0.25, and 0.5 on a cubic lattice. The magnitude of the nearest-neighbor component of the electron-phonon interaction has been shown in both one and two dimensions to be the most significant contributing factor to bipolaron properties.[7,8] The simulation produces exact numerical solutions for the total energy, average number of excited phonons, mass, and size of singlet bipolarons.

In the following, we examine only the singlet bipolaron for a range of U/t and λ at inverse temperature $\bar{\beta} = 14$ with fixed $\hbar\omega/\mathrm{W} = 1$, where the half-bandwidth $\mathrm{W} = 6t$, which is towards the lower end of the intermediate phonon frequency limit. Calculations are carried out on an infinite lattice where particles are confined to within 50 lattice spacings of each other, which is sufficiently large to avoid the majority of finite-size effects. The most sensitive property to finite-size effects is the bipolaron radius, which does not become infinite when the polarons are not bound into a bipolaron. All errors are determined using bootstrap resampling on the simulation data and are displayed as three standard errors.

The binding of bipolarons can be established from the total energy. Figure 1(a) depicts the total energy calculated from our Monte Carlo calculations when $\gamma = 0$ (Holstein interaction). Diagonal lines show the presence of pairs of electrons on a single site. As the Hubbard onsite repulsion U is increased, the onsite pairs are pushed apart creating pairs of polarons. As the electron-phonon coupling constant λ is increased, we see that larger Hubbard U is needed to break apart the onsite pairs. When the pair is unbound, the energy of the bipolaron does not change with respect to increasing U, and the line is horizontal. A key difference here is that it takes a large negative Hubbard U to bind onsite bipolarons in contrast to 1D and 2D systems.

Plots of the total energy of the bipolaron formed when the electron-phonon interaction contains a nearest-neighbor component of $\gamma = 0.25$ and 0.5 are also shown [Figs. 1(b) and 1(c), respectively]. It is immediately apparent that the rapid transition from onsite bipolaron to free polarons is smoothed out with the addition of nearest-neighbor interaction. There is no dramatic change between the total energy of the Holstein and extended Holstein bipolarons for electron-phonon coupling $\lambda = 0.2$, as there is insufficient intersite interaction to bind an off-site bipolaron. This is in contrast to 1D and 2D where significant qualitative changes to all bipolaron properties are found when intersite interaction is switched on.

We observe that the U value corresponding to the point of inflection is reduced with increasing γ. This does not correspond to bipolarons which are more weakly bound (i.e., easier to unbind when the Hubbard U is switched on). Rather, as electron-phonon coupling is increased, the crossover from bound pairs to unbound pairs occupies a wider range of U

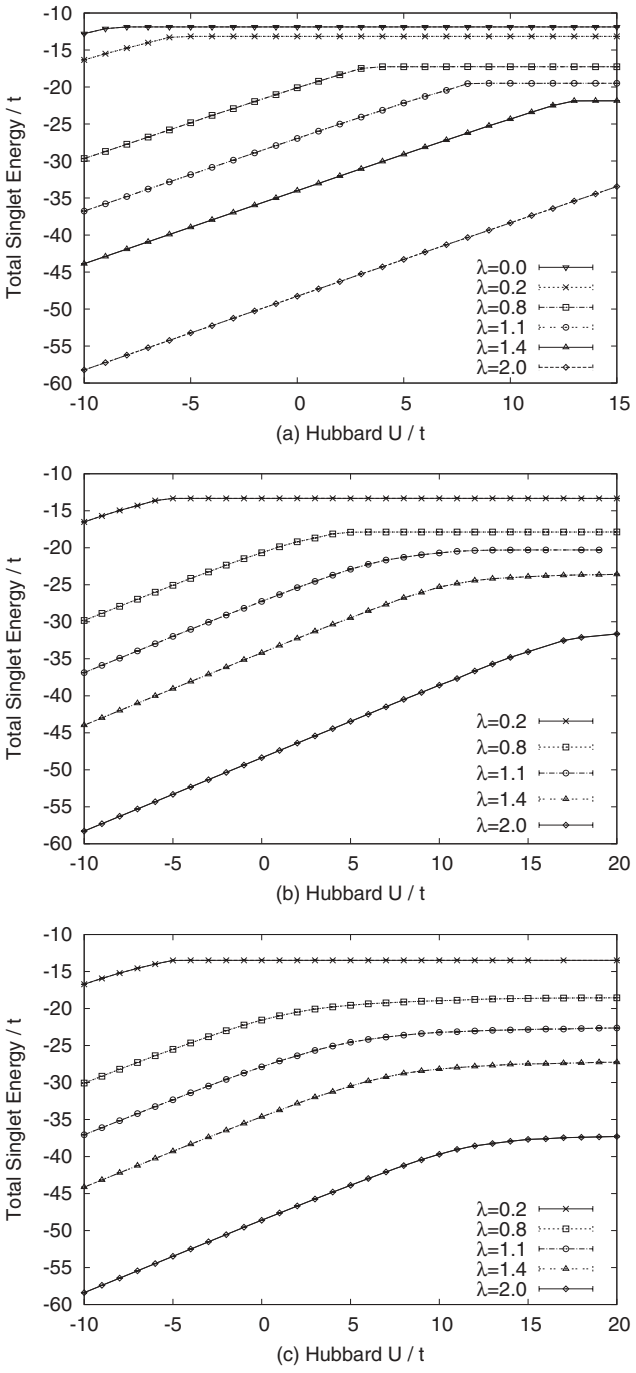

FIG. 1. Total ground state energy simulated by CTQMC of (a) a singlet Hubbard-Holstein bipolaron (b) singlet bipolaron with nearest-neighbor interaction strength of $\gamma = 0.25$ and (c) $\gamma = 0.5$. Similar to large phonon frequency (see Appendix), it takes significant negative Hubbard U to bind onsite bipolarons. For large intersite interaction and large λ, a crossover is seen between onsite and intersite bipolarons.

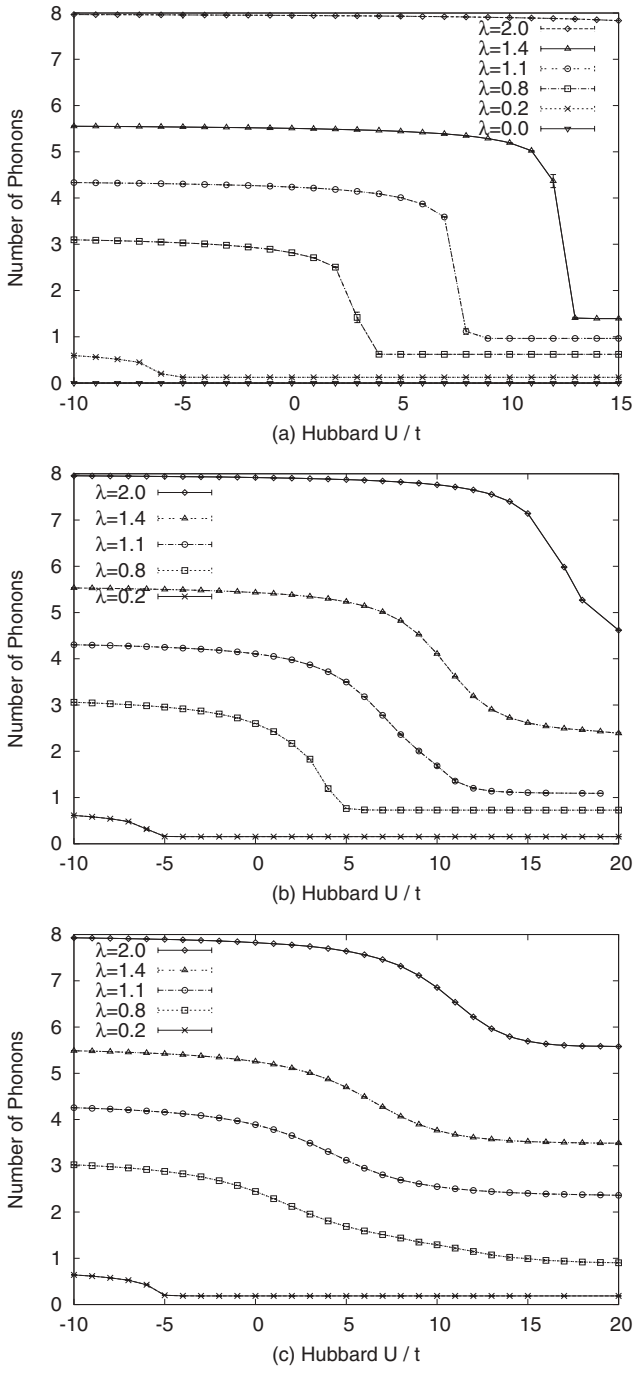

FIG. 2. Number of phonons associated with (a) a singlet Hubbard-Holstein bipolaron, and (b) bipolarons with nearest-neighbor interaction strength of $\gamma = 0.25$ and (c) $\gamma = 0.5$. Again, the range of crossover between onsite bipolaron and unbound/intersite bipolarons increases with γ.

values. Comparison with Fig. 1(a) shows that total energy at large U typically decreases with increased nearest-neighbor attraction, consistent with this observation.

Further evidence for binding of bipolarons can be found in the total number of excited phonons shown in Fig. 2. Here, we see that at large Hubbard U, the number of phonons in the system does not change with respect to U, although it is nonzero, because even unbound polarons have phonons associated with them. This can be seen in Fig. 2(a), the Holstein case, as λ increases from $\lambda = 0$ (where there are no phonons) to higher phonon coupling, where there are a significant number of residual phonons at high U. The curve showing the total number of phonons also levels out at large U when there is significant intersite coupling and bipolarons large but bound,

which occurs because there is vanishing onsite component of the wave function in the presence of sufficient U and therefore the system is unchanged as U is varied.

On lowering U in Fig. 2(a), we see that the number of phonons associated with the bipolaron rapidly increases as the onsite bipolaron forms. This is due to the rapid crossover from unbound or intersite pairs to onsite pairs. As U decreases further, the number of phonons tends again to a set value dictated by the electron-phonon coupling constant and phonon frequency, which also does not depend on U. This occurs at sufficient negative U where the bipolaron is forced into an onsite configuration. Plots for $\gamma = 0.25$ and 0.5 are shown in Figs. 2(b) and 2(c) for the extended Holstein case. Again, an increase in nearest-neighbor attractive potential visibly smooths out transition from bound pairs at low U and the unbound or offsite pairs seen at large U. The crossover from bound to unbound is stretched over a larger range of U consistent with the similar observation in the total energy. With increased nearest-neighbor attraction, the number of associated phonons decreases less dramatically as onsite pairs form, presumably because an increased number of phonons are associated with the intersite pairs.

It is of particular interest to examine the change in singlet bipolaron inverse mass as U and λ are varied, as this can be related to the BEC transition temperature. Figure 3 shows that the mass is near constant at large U. Bound onsite pairs have a high mass (low inverse mass). The inverse mass rapidly decreases at the point of binding. We see that the transition from bipolaron to polaron starts at lower U, with increased nearest-neighbor interaction [Figs. 3(b) and 3(c)]. The mass decreases more slowly with increased Hubbard U for a higher interaction in accordance with the slow change in associated phonons. With high coupling constant $\lambda \gtrsim 1.1$ and $\gamma = 0.5$, we see that the inverse mass has a maximum before decreasing and then leveling off, showing that the effective mass has a minimum value at intermediate U. This phenomenon is not clearly visible in the total energy. The reduction in mass is a version of the superlight small bipolaron behavior[4,7,8,31] and is achieved when onsite and intersite interactions become comparable in size so that bipolarons can hop by contracting and expanding through degenerate onsite to intersite pairs without energy penalty. This behavior is significant because small mobile bipolarons could form a Bose-Einstein condensate with significant transition temperature. We will discuss this possibility in the next section.

Wave functions of individual pairs may not overlap if bipolarons are to be well defined, so the bipolaron size limits the maximum density of particles in a bipolaronic material. Figure 4 plots the inverse average singlet bipolaron size against the Hubbard U. Figure 4(a) shows the inverse bipolaron size for the local Holstein interaction. As expected for large U, bipolaron pairs unbind and the bipolaron size becomes infinite. With increasing coupling constant λ, the average bipolaron size becomes smaller (inverse size plotted) as the attractive phonon-mediated interactions overcome the repulsive Hubbard U.

In Figs. 4(b) and 4(c), where intersite interaction is turned on, qualitatively different behavior of the bipolaron size can be seen. For weak electron-phonon coupling $\lambda \lesssim 1$, we see that inverse bipolaron size tends to zero at high Hubbard U.

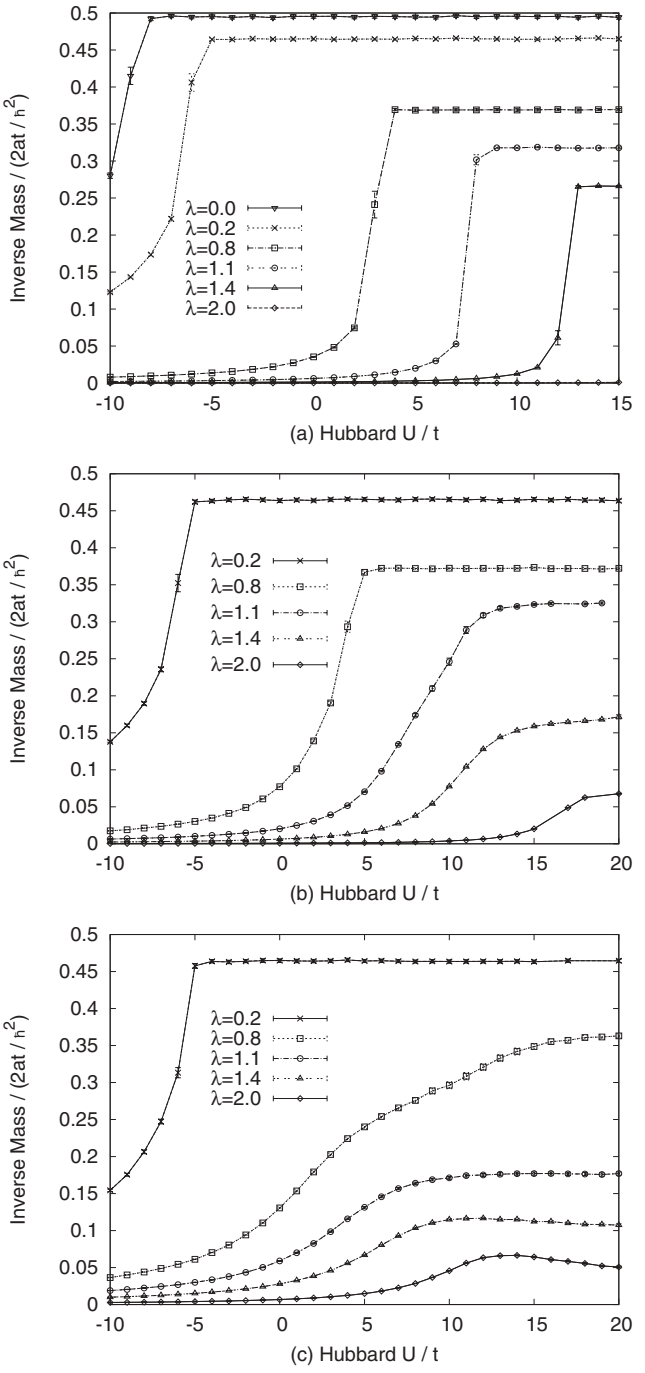

FIG. 3. Inverse mass of the singlet bipolaron with nearest-neighbor interaction for interaction strength of (a) $\gamma = 0$, (b) $\gamma = 0.25$, and (c) $\gamma = 0.5$. For large coupling constant $\lambda \gtrsim 1.1$ and $\gamma = 0.5$, we see that the inverse mass has a maximum before decreasing and then leveling off. The reduction in mass is a version of the superlight small bipolaron behavior, and is achieved when onsite and intersite interactions become comparable. Light mobile bipolarons may form a BEC with significant transition temperature.

The value of U required for unbinding increases with γ. With large intersite interaction of $\gamma = 0.5$, we see that bipolaron unbinding does not occur at high U for coupling constant $\lambda \gtrsim 1.1$ (within the range investigated), instead tending towards a bipolaron size on the order of a lattice constant. At $\lambda =$

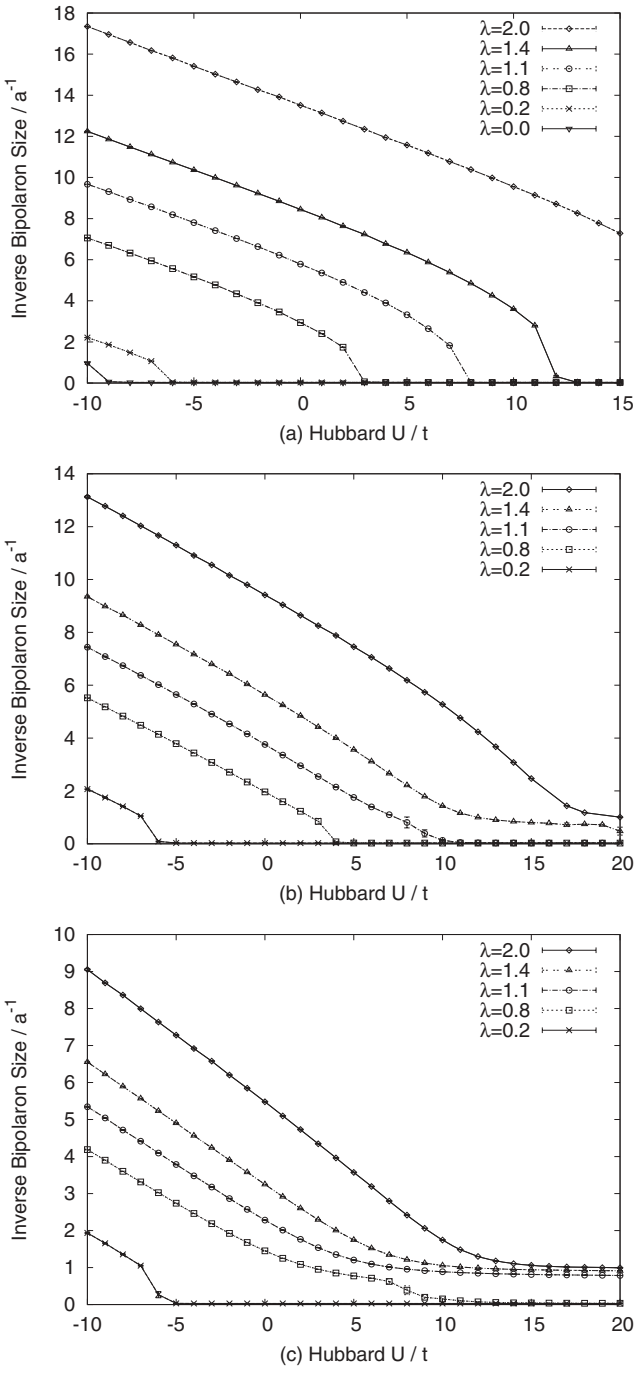

FIG. 4. Singlet bipolaron inverse size with nearest-neighbor interaction strength of (a) $\gamma = 0$, (b) $\gamma = 0.25$, and (c) $\gamma = 0.5$. At $\lambda = 0.8$ and $\gamma = 0.5$, an inflection in the bipolaron size shows the transition of onsite bound pairs through intersite pairing before the bipolaron completely unbinds on increasing U. This is the precursor of the superlight bipolaron behavior found at larger λ.

0.8 and $\gamma = 0.5$, an inflection in the bipolaron size shows the crossover from onsite bound pairs through off-site pairing before the bipolaron completely unbinds on increasing U. This is the precursor of the superlight bipolaron behavior found at larger λ.

We conclude this section by examining the infinite Hubbard U case. Figure 5 displays inverse bipolaron size against

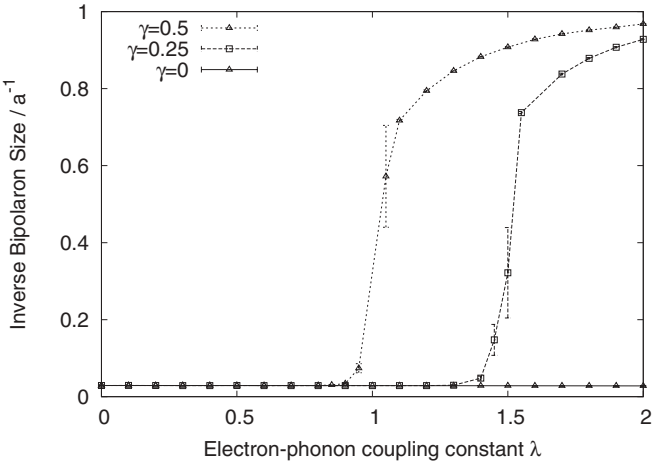

FIG. 5. Singlet bipolaron inverse size with increasing electron phonon coupling for infinite Hubbard U, showing the transition from unbound to bound states. Nearest-neighbor strength $\gamma = 0$, 0.25, and 0.5. Intersite bound pairs are shown seen to exist at large λ when nearest-neighbor interactions are switched on.

increasing electron-phonon coupling constant with nearest-neighbor interaction strength $\gamma = 0$, 0.25, and 0.5, showing the crossover from unbound states to bound intersite pairs. It is seen that for $\gamma = 0.25$ and 0.5, the system is never fully unbound above $\lambda \simeq 1.5$ and 1, respectively. Both have a sharp decrease of bipolaron size that tends to a value equal to one lattice spacing. Intersite bound pairs are therefore shown to exist at large U and λ when nearest-neighbor interactions are switched on.

IV. BOSE-EINSTEIN CONDENSATION

Evidence from the quantum Monte Carlo simulations presented in the previous section shows that 3D bipolarons can be simultaneously small and light in the region of the parameter space where perturbation theory breaks down. In this section, we examine if bosonic charge carriers of this type could form a Bose-Einstein condensate (BEC) with a significant transition temperature.

The BEC transition temperature can be calculated using the expression

$$k_{\mathrm{B}} T_{\mathrm{BEC}} = \frac{3.31\hbar^2}{m^{**}} \left(\frac{n_b}{a^3}\right)^{2/3}, \tag{10}$$

where n_b is the number of bosons per site, m^{**} is the effective boson mass, and a is the lattice constant (here we take a to be 4.2 Å, consistent with the bismuthates). An upper bound on the number of bosons per lattice site can be established by utilizing the bipolaron size R, $n_b/a^3 \approx 1/R'^3$, where R' is the effective radius of the bipolaron. From this, we get the following relation:

$$T_{\mathrm{BEC}} = \frac{3.31\hbar^2}{k_{\mathrm{B}} m^{**} R'^2}. \tag{11}$$

Figure 6 is a plot of transition temperatures with (a) Holstein and intersite interaction strengths (b) $\gamma = 0.25$ and (c) $\gamma = 0.5$. We only plot positive Hubbard U in this section since

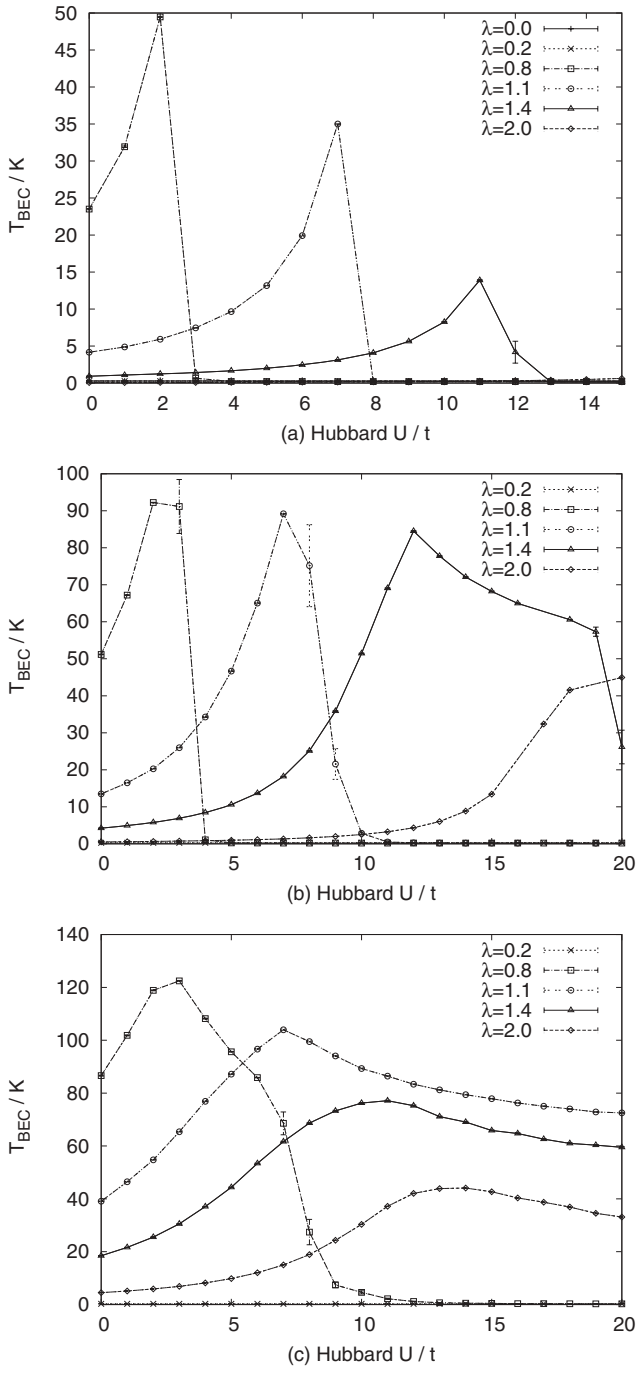

FIG. 6. BEC transition temperature with nearest-neighbor interaction strength of (a) $\gamma = 0$, (b) $\gamma = 0.25$, and (c) $\gamma = 0.5$. The divergence in T_{BEC} for the Holstein case will be suppressed because the bipolaron is only weakly bound. On the other hand, high transition temperatures of 90–120 K are seen with nearest-neighbor interaction strength $\gamma = 0.5$ and medium electron-phonon coupling constant where bipolarons are well bound.

negative U would be unphysical. The effective radius R' is taken to be $5R$ (a bipolaron separation is 5 bipolaron radii in each direction) corresponding to a bipolaron wave-function overlap of less than 1%. As bipolaron densities increase so that bipolarons overlap, interaction corrections are expected to reduce transition temperatures.

Several sharp peaks in T_{BEC} are seen in Fig. 6(a) for Holstein electron-phonon coupling constants of $\lambda = 0.8$, 1.1 and 1.4 (for weaker λ, the peaks are at unphysical negative U values). These peaks reach values temperatures of ~50 K. The regions of high T_{BEC} are unstable to small variation in U and bipolarons are only weakly bound, so thermal fluctuations will suppress transition temperatures by breaking up the bipolaron. For weak electron-phonon coupling, bipolarons only bind at unphysical negative U values, and no BEC is formed for positive U. It is interesting to note that although bipolarons are formed through electron-phonon coupling, there is a wide region of the parameter space where increasing the Hubbard U raises the transition temperature.

BEC transition temperatures are shown for nearest-neighbor interaction $\gamma = 0.25$ in Fig. 6(b). Similar to the Holstein case, T_{BEC} has a peak at low Hubbard U for intermediate λ. The peak width increases with electron-phonon coupling, but the maximum in the transition temperature decreases slightly. A tail appears at large U for coupling constant $\lambda = 1.4$, where the bipolaron becomes bound between sites and properties depend only weakly on U. QMC simulations are essential here since the regions of high transition temperature (where both the electron-phonon coupling and Hubbard U are intermediate) can not be accessed using perturbative techniques.

Finally, Fig. 6(c) plots BEC transition temperatures for nearest-neighbor interaction strength $\gamma = 0.5$. The strong intersite coupling completely eradicates the sharp peaks in transition temperature associated with the Holstein interaction, replacing them with broad continuous curves with increased T_{BEC}. Bipolarons with medium to high λ form stable nearest-neighbor pairs with low effective masses, leading to superconducting states that have significant transition temperatures over wide range of U. Bipolarons formed from large electron-phonon coupling have larger effective masses, leading to significantly lower condensation temperatures. The most interesting point here is that for medium-sized coupling constants, bipolaron effective masses are still small when bipolarons are bound into small intersite pairs, resulting in high condensation temperatures of 90–120 K. Note that the use of R' leads to an approximation on the possible T_{BEC}, lower transition temperatures are estimated if the upper bound on the distance between bipolarons is larger (before inter-boson interactions need to be taken into account), and interactions between bipolarons typically lower transition temperatures. Again, it is interesting to note that the BEC transition temperature can increase as U increases, even though the mechanism for binding pairs is phonon mediated. Since bipolarons are bound at very large U and λ (as shown in Fig. 4), no breakdown of the BEC is seen for very large repulsive Coulomb interactions, and the transition temperature remains significant. This is important because many oxide materials with large electron-phonon interactions also have large U.

To probe the sensitivity of bipolarons to impurities, we calculate the effective hopping for the bipolarons,

$$t' = \frac{\hbar^2}{2a^2 m^{**}}. \tag{12}$$

Figure 7 shows the effective bipolaron hopping energy when $\gamma = 0.5$. For electron-phonon coupling constants $\lambda = 1.1$

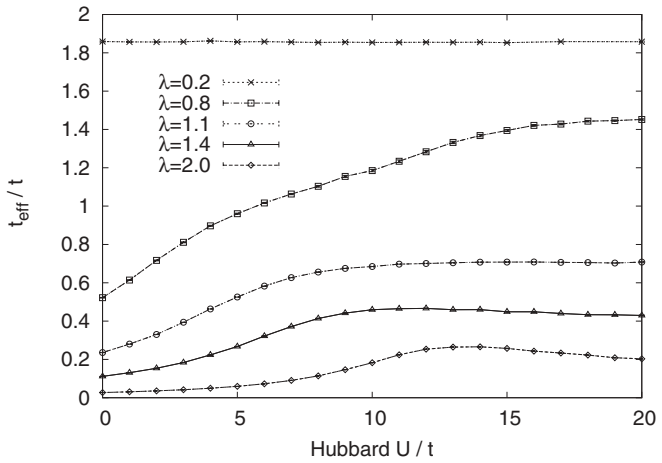

FIG. 7. Effective Hopping energies with nearest-neighbor interaction strength of $\gamma = 0.5$. Bipolarons with medium electron-phonon coupling λ are shown to be mobile with effective hopping energies in the region of the bare hopping energy.

and 1.4, bipolarons have an effective hopping $t_{\rm eff} \approx 0.7t$ and $0.4t$, respectively. As we have previously shown,[7] local impurities with energy $\Delta = -4t_{\rm eff}$ are needed to pin polarons to impurities. Therefore, for any reasonable impurity size, bipolarons are mobile.

V. SUMMARY AND CONCLUSIONS

We have investigated the formation of bipolarons and their subsequent Bose-Einstein condensation on a three-dimensional cubic lattice. A quantum Monte Carlo code was employed to investigate regimes of intermediate electron-phonon coupling and Coulomb repulsion, and was validated using analytic calculations in the large phonon frequency limit. Away from the regions where perturbation theories are valid, the effective mass and bipolaron radius are consistent with light small bipolarons.

A consequence of the 3D lattice is that binding of bipolarons is difficult for weak λ. Small and mobile bipolarons form for intermediate λ and intersite coupling γ when the energies of onsite and intersite pairs become similar. By analyzing the exact numerical results, we have shown that bipolaron condensation temperatures (leading to superconductivity) could be up to 90–120 K for realistic bipolaron densities. Another consequence of 3D is that it is more difficult to bind bipolarons to impurities. Impurity energies of around $-4t_{\rm eff}$ are required to localize particles in 3D. Therefore, the light bipolaron states are stable against attractive impurity levels with energies of up to $\sim t$ as the effective hopping has a similar magnitude to the bare electron hopping energy. We conclude that stable bipolaron superconductors that are insensitive to changes in Hubbard U could form in three-dimensional oxides with intersite electron-phonon interactions of intermediate magnitude (that is, electron-phonon interactions with a moderate momentum dependence). Moreover, with sufficiently large intersite electron-phonon coupling, superconductivity could be stable at very large values of U, demonstrating that Coulomb repulsion is no barrier to bipolaronic superconductivity in 3D.

ACKNOWLEDGMENTS

We are pleased to thank A. Umerski, S. Alexandrov, and J. Samson for useful discussions. J.P.H. would like to acknowledge EPSRC Grant No. EP/H015655/1.

APPENDIX: HIGH PHONON FREQUENCY AND THE UV MODEL

The bipolaron properties can be analytically approximated in the high phonon frequency (antiadiabatic) limit ($\hbar\omega \gg W$) by using the result of the Lang-Firsov transformation since if the phonon frequency is very large, there are no real phonons. Up to a linear shift in energy, the resulting U-V model is shown as

$$\tilde{H} = -\sum_{nn'\sigma} t'_{nn'} c^\dagger_{n\sigma} c_{n'\sigma} + U' \sum_n c^\dagger_{n\uparrow} c_{n\uparrow} c^\dagger_{n\downarrow} c_{n\downarrow} + {\sum_{nn'}}' \sum_{\sigma\sigma'} V'_{nn'} c^\dagger_{n\sigma} c_{n\sigma} c^\dagger_{n'\sigma'} c_{n'\sigma'}. \quad \text{(A1)}$$

The primed sum over V' in the final part of Eq. (A1) ignores the self-interaction term. The interaction terms in this Hamiltonian for onsite interaction and nearest-neighbor interactions are $U' = U - 2W\lambda$ and $V'_{nn'} = 2W\lambda\Phi_0(n,n')/\Phi_0(0,0)$, respectively.

Taking the two-particle Schrödinger equation

$$[E - \epsilon(\boldsymbol{k}_1) - \epsilon(\boldsymbol{k}_2)]\chi(\boldsymbol{k}_1,\boldsymbol{k}_2) = U' \sum_{\boldsymbol{q}} \chi(\boldsymbol{q}, \boldsymbol{k}_1 + \boldsymbol{k}_2 - \boldsymbol{q}) - V' \sum_{\boldsymbol{l}} e^{-i\boldsymbol{k}_1\cdot\boldsymbol{l}} \sum_{\boldsymbol{q}} \chi(\boldsymbol{q}, \boldsymbol{k}_1 + \boldsymbol{k}_2 - \boldsymbol{q}) e^{i\boldsymbol{q}\cdot\boldsymbol{l}}, \quad \text{(A2)}$$

$$\epsilon(\boldsymbol{k}) = -t' \sum_{\boldsymbol{l}} e^{-i\boldsymbol{k}\cdot\boldsymbol{l}} = -2t'(\cos\boldsymbol{k}_x + \cos\boldsymbol{k}_y + \cos\boldsymbol{k}_z), \quad \text{(A3)}$$

where $\boldsymbol{l} = \{(\pm1,0,0),(0,\pm1,0),(0,0,\pm1)\}$ assuming that the lattice constant $a = 1$ (this will be assumed throughout). To simplify the problem, we introduce a set of momentum-dependent values $\Delta(\boldsymbol{K})$:

$$\Delta_{(0,0,0)}(\boldsymbol{K}) \equiv \sum_{\boldsymbol{q}} \chi(\boldsymbol{q}, \boldsymbol{k}_1 + \boldsymbol{k}_2 - \boldsymbol{q}), \quad \text{(A4)}$$

$$\Delta_{\boldsymbol{l}}(\boldsymbol{K}) \equiv \sum_{\boldsymbol{q}} \chi(\boldsymbol{q}, \boldsymbol{k}_1 + \boldsymbol{k}_2 - \boldsymbol{q}) e^{i\boldsymbol{q}\cdot\boldsymbol{l}}, \quad \text{(A5)}$$

and then substitute them into the Schrödinger equation (A2). By rearranging the resulting equation, we obtain an expression for χ in terms of $\boldsymbol{K}$ and $\boldsymbol{q}$, where $\boldsymbol{K} = \boldsymbol{k}_1 + \boldsymbol{k}_2$:

$$\chi(\boldsymbol{k}_1,\boldsymbol{k}_2) = \frac{U'\Delta_{(0,0,0)}(\boldsymbol{K}) - V' \sum_{\boldsymbol{l}} \Delta_{\boldsymbol{l}}(\boldsymbol{K}) e^{-i\boldsymbol{k}_1\cdot\boldsymbol{l}}}{E - \epsilon(\boldsymbol{k}_1) - \epsilon(\boldsymbol{k}_2)}, \quad \text{(A6)}$$

$$\chi(\boldsymbol{q}, \boldsymbol{K} - \boldsymbol{q}) = \frac{U'\Delta_{(0,0,0)}(\boldsymbol{K}) - V' \sum_{\boldsymbol{l}} \Delta_{\boldsymbol{l}}(\boldsymbol{K}) e^{-i\boldsymbol{q}\cdot\boldsymbol{l}}}{E - \epsilon(\boldsymbol{q}) - \epsilon(\boldsymbol{K} - \boldsymbol{q})}. \quad \text{(A7)}$$

Expanding the expression for $\chi(\boldsymbol{q},\boldsymbol{K}-\boldsymbol{q})$ from Eq. (A7) into a matrix format leads to the following relation:

$$\begin{pmatrix} L_0-\frac{1}{U'} & L_{-x} & L_x & L_{-y} & L_y & L_{-z} & L_z \\ L_x & L_0+\frac{1}{V'} & L_{2x} & L_{x-y} & L_{x+y} & L_{x-z} & L_{x+z} \\ L_{-x} & L_{-2x} & L_0+\frac{1}{V'} & L_{-x-y} & L_{-x+y} & L_{-x-z} & L_{-x+z} \\ L_y & L_{y-x} & L_{y+x} & L_0+\frac{1}{V'} & L_{2y} & L_{y-z} & L_{y+z} \\ L_{-y} & L_{-y-x} & L_{-y+x} & L_{-2y} & L_0+\frac{1}{V'} & L_{-y-z} & L_{-y+z} \\ L_z & L_{z-x} & L_{z+x} & L_{z-y} & L_{z+y} & L_0+\frac{1}{V'} & L_{2z} \\ L_{-z} & L_{-z-x} & L_{-z+x} & L_{-z-y} & L_{-z+y} & L_{-2z} & L_0+\frac{1}{V'} \end{pmatrix} \begin{pmatrix} U'\Delta_{(0,0,0)} \\ -V'\Delta_x \\ -V'\Delta_{-x} \\ -V'\Delta_y \\ -V'\Delta_{-y} \\ -V'\Delta_z \\ -V'\Delta_{-z} \end{pmatrix} = 0, \tag{A8}$$

$$L_p = L_{q_p}(E,\boldsymbol{K}) = \sum_{\boldsymbol{q}} \frac{e^{iq_p}}{E-\epsilon(\boldsymbol{q})-\epsilon(\boldsymbol{K}-\boldsymbol{q})}. \tag{A9}$$

At the Γ point, $\boldsymbol{K}=(0,0,0)$, the additional symmetry simplifies analysis of Eq. (A8) since Eq. (A9) can be reduced to the following components: $L_{\pm x}=L_{\pm y}=L_{\pm z}\equiv L_1$, $L_{\pm 2x}=L_{\pm 2y}=L_{\pm 2z}\equiv L_2$, and $L_{\pm x\pm y}=L_{\pm y\pm z}=L_{\pm z\pm x}\equiv L_3$.

To diagonalize the problem, a new basis of states with s-, p-, and d-wave symmetry is introduced:

$$\begin{aligned} &\Delta_0=\Delta_{(0,0,0)}, \quad \Delta_s=\frac{1}{\sqrt{6}}(\Delta_x+\Delta_{-x}+\Delta_y+\Delta_{-y}+\Delta_z+\Delta_{-z}), \quad \Delta_{p_1}=\frac{1}{\sqrt{2}}(\Delta_x-\Delta_{-x}), \\ &\Delta_{p_2}=\frac{1}{\sqrt{2}}(\Delta_y-\Delta_{-y}), \quad \Delta_{p_3}=\frac{1}{\sqrt{2}}(\Delta_z-\Delta_{-z}), \quad \Delta_{d_1}=\frac{1}{\sqrt{4}}(\Delta_x+\Delta_{-x}-\Delta_y-\Delta_{-y}), \\ &\Delta_{d_2}=\frac{1}{\sqrt{12}}(\Delta_x+\Delta_{-x}+\Delta_y+\Delta_{-y}-2\Delta_z-2\Delta_{-z}), \end{aligned} \tag{A10}$$

where the s and d states are symmetric and p states antisymmetric on inversion through the origin.

Applying the new basis of Δ's to the matrix equation leads to a simple block-diagonal matrix consisting of two s states (Δ_0 and Δ_s), three p, and two d states:

$$\begin{pmatrix} L_0-\frac{1}{U'} & 6L_1 & 0 & 0 & 0 & 0 & 0 \\ L_1 & L_S+\frac{1}{V'} & 0 & 0 & 0 & 0 & 0 \\ 0 & 0 & \lambda_p & 0 & 0 & 0 & 0 \\ 0 & 0 & 0 & \lambda_p & 0 & 0 & 0 \\ 0 & 0 & 0 & 0 & \lambda_p & 0 & 0 \\ 0 & 0 & 0 & 0 & 0 & \lambda_d & 0 \\ 0 & 0 & 0 & 0 & 0 & 0 & \lambda_d \end{pmatrix} \begin{pmatrix} U'\Delta_0 \\ -V'\Delta_s \\ -V'\Delta_{p_1} \\ -V'\Delta_{p_2} \\ -V'\Delta_{p_3} \\ -V'\Delta_{d_1} \\ -V'\Delta_{d_2} \end{pmatrix}, \tag{A11}$$

where

$$\begin{aligned} L_0 &= \sum_{\boldsymbol{q}} \frac{1}{E-2\epsilon(\boldsymbol{q})}, \\ L_S &= \sum_{\boldsymbol{q}} \frac{2\cos q_x(\cos q_x+\cos q_y+\cos q_z)}{E-2\epsilon(\boldsymbol{q})}, \\ \lambda_p &= L_0+\frac{1}{V'}-L_2, \\ \lambda_d &= L_0+\frac{1}{V'}+L_2-2L_3. \end{aligned} \tag{A12}$$

The p and d states are diagonalized in the new basis and their energies can be calculated directly from

$$\begin{aligned} \lambda_p &= 0, \\ \lambda_d &= 0. \end{aligned} \tag{A13}$$

The ground-state singlet states can be computed from solution of the 2×2 matrix in the top left-hand corner of Eq (A11):

$$\begin{pmatrix} L_0-\frac{1}{U'} & 6L_1 \\ L_1 & L_S+\frac{1}{V'} \end{pmatrix} \begin{pmatrix} U'\Delta_0 \\ -V'\Delta_s \end{pmatrix} = 0, \tag{A14}$$

which can be used to calculate energies of the s state by taking the determinant

$$\left(L_0-\frac{1}{U'}\right)\left(L_S+\frac{1}{V'}\right)-6L_1^2=0. \tag{A15}$$

Rearranging Eq. (A15),

$$L_0=\frac{V'\left(6U'L_1^2+L_S\right)+1}{U'(V'L_S+1)}, \tag{A16}$$

a binary search can be used to determine values of E for various values of U' and V'.

The solutions found by this method are shown in Fig. 8. Typically, there is a smooth transition from bound states

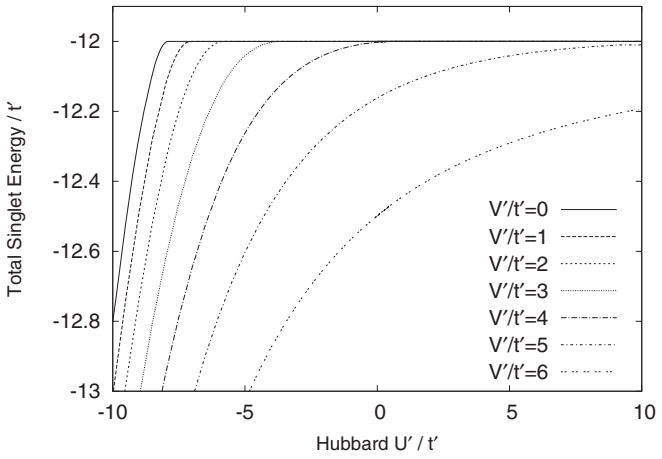

FIG. 8. Ground-state bipolaron singlet energy computed for a UV model on a cubic lattice. A key result here is that it takes a large negative Hubbard U to bind onsite bipolarons in contrast to 1D and 2D systems. At low V', the bipolaron binds for finite U, but for large V', the unbinding occurs at very large (infinite) U since the intersite bipolaron is stable.

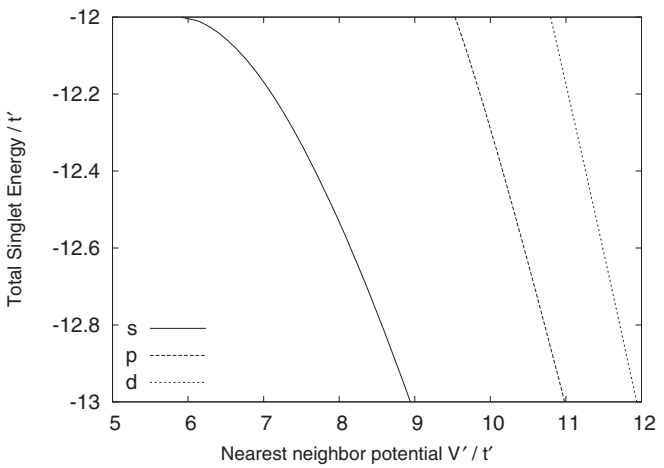

FIG. 9. Exact bipolaron energy computed for a U-V model on a cubic lattice. Here, we examine the energy at infinite U' to observe if there is a critical V' that ensures binding in the 3D lattice for s, p, and d states.

(diagonal lines) to unbound states (horizontal lines). For $V = 0$, the graph depicts a diagonal line with constant gradient representing a bound onsite pair that at about $U'/t' \simeq -8$ levels off to a horizontal line representing unbound polarons in the lattice. With increasing nearest-neighbor potential V', the transition from bound to unbound states spans a larger range of Hubbard U' (curved line), and is related to the presence of intersite pairs in the lattice. At large enough V', there are no unbound states.

Even if there is no intersite repulsion $V'/t' = 0$, strong negative Hubbard values $U'/t' = -7.915$ are required to bind the bipolaron in contrast to 1D and 2D lattices where you need $U'/t' = 0$.[7,8] This is due to the additional degrees of freedom in the cubic structure, where electrons are not confined in any direction. For a nearest-neighbor attraction of $V'/t' = 4$, Fig. 8 shows that binding occurs around $U' = 0$ (actual crossing value $V'/t' = 3.875$), whereas on the square lattice the presence of V'/t' leads to off-site pairing at strong positive U'. The lack of confinement in 3D means that bipolaron onsite pairing is not guaranteed even with high coupling constants. Applying a small nearest-neighbor potential in 2D has a much bigger effect on the binding than in 3D due to the confinement.[8]

To understand the qualitative difference in bipolaron behavior as V' is changed, we evaluated the energy of the pair at infinite U. In Fig. 9, we plot the total energy [from Eq. (A16)] as a function of nearest-neighbor potential V', showing the binding of the s state as V' is increased. We also show both p and d states for completeness. For the s state, the binding crossover begins at a nearest-neighbor interaction strength of $V'/t' = 5.875$. After this point, the energy curves sharply to an approximate $E \propto V'$ for high V'. The energies of the p and d states do not level off at $E = -12t'$ since they are excited states.

[1] A. Alexandrov and J. Ranninger, Phys. Rev. B **24**, 1164 (1981).
[2] D. Emin, Phys. Rev. Lett. **62**, 1544 (1989).
[3] A. S. Alexandrov, *Polarons in Advanced Materials* (Springer, New York, 2007).
[4] J. P. Hague, P. E. Kornilovitch, J. H. Samson, and A. S. Alexandrov, Phys. Rev. Lett. **98**, 037002 (2007).
[5] A. Schirotzek, C.-H. Wu, A. Sommer, and M. W. Zwierlein, Phys. Rev. Lett. **102**, 230402 (2009).
[6] L. Landau, Phys. Z. Sowjetunion **3**, 664 (1933).
[7] J. P. Hague and P. E. Kornilovitch, Phys. Rev. B **80**, 054301 (2009).
[8] J. P. Hague and P. E. Kornilovitch, Phys. Rev. B **82**, 094301 (2010).
[9] J. Bonča and S. A. Trugman, Phys. Rev. B **64**, 094507 (2001).
[10] A. S. Alexandrov and P. E. Kornilovitch, J. Phys.: Condens. Matter **14**, 5337 (2002).
[11] G. Wellein, H. Röder, and H. Fehske, Phys. Rev. B **53**, 9666 (1996).
[12] I. B. Bischofs, V. N. Kostur, and P. B. Allen, Phys. Rev. B **65**, 115112 (2002).
[13] *Physics of Organic Semiconductors,* edited by W. Brütting (Wiley-VCH, Weinheim, 2005).
[14] M. A. Smondyrev, E. A. Kochetov, G. Verbist, F. M. Peeters, and J. T. Devreese, Europhys. Lett. **19**, 519 (1992).
[15] A. Weiße, H. Fehske, G. Wellein, and A. R. Bishop, Phys. Rev. B **62**, R747 (2000).
[16] J. Bonča, T. Katrašnik, and S. A. Trugman, Phys. Rev. Lett. **84**, 3153 (2000).
[17] E. Jeckelmann, C. Zhang, and S. R. White, Phys. Rev. B **60**, 7950 (1999).
[18] M. Hohenadler and W. von der Linden, Phys. Rev. B **71**, 184309 (2005).
[19] B. Y. Yavidov, Eur. Phys. J. B **75**, 481 (2010).

[20] A. Macridin, G. A. Sawatzky, and M. Jarrell, Phys. Rev. B **69**, 245111 (2004).
[21] S. Sil, A. K. Giri, and A. Chatterjee, Phys. Rev. B **43**, 12642 (1991).
[22] G. Verbist, F. M. Peeters, and J. T. Devreese, Phys. Rev. B **43**, 2712 (1991).
[23] R. Yong-Hong and C. Qing-Hu, Commun. Theor. Phys. **48**, 169 (2007).
[24] Chen Qinghu, Wang Kelin, and W. Shaolong, Phys. Rev. B **50**, 164 (1994).
[25] N. I. Kashirina and V. D. Lakhno, Phys.-Usp. **53**, 431 (2010).
[26] V. K. Mukhomorov, Phys. Scr. **69**, 139 (2004).
[27] J. P. Hague, P. E. Kornilovitch, and A. S. Alexandrov, Phys. Rev. B **78**, 092302 (2008).
[28] J. Hubbard, Proc. R. Soc. A **276**, 238 (1963).
[29] I. G. Lang and Y. A. Firsov, Zh. Eksp. Teor. Fiz. **43** 1843 (1962) [Sov. Phys.–JETP **16**, 1301 (1963)].
[30] P. E. Kornilovitch, Phys. Rev. Lett. **81**, 5382 (1998).
[31] J. Hague, P. Kornilovitch, J. Samson, and A. Alexandrov, J. Phys.: Condens. Matter **19**, 255214 (2007).